‖‖‖‖‖‖‖‖‖‖‖‖‖‖‖‖‖‖‖‖

# The Modal Decomposition
# of an Impedance Tube

Andrew J. Hull
Submarine Sonar Department

DTIC
ELECTE
AUG 2 3 1994
S B D

94-26791

‖‖‖‖‖‖‖‖‖‖‖‖‖‖‖‖‖‖‖‖‖‖‖

# Naval Undersea Warfare Center Division
## Newport, Rhode Island

94 8 22 1 80

# PREFACE

REVIEWED AND APPROVED: 8 JUNE 1994

W. J. Coggins
Acting Head, Submarine Sonar Department

# REPORT DOCUMENTATION PAGE

Public reporting burden for this collection of information is estimated to average 1 hour per response, including the time for reviewing instructions, searching existing data sources, gathering and maintaining the data needed, and completing and reviewing the collection of information. Send comments regarding this burden estimate or any other aspect of this collection of information, including suggestions for reducing this burden, to Washington Headquarters Services, Directorate for Information Operations and Reports, 1215 Jefferson Davis Highway, Suite 1204, Arlington, VA 22202-4302, and to the Office of Management and Budget, Paperwork Reduction Project (0704-0188), Washington, DC 20503.

| 1. AGENCY USE ONLY (Leave Blank) | 2. REPORT DATE | 3. REPORT TYPE AND DATES COVERED |
|---|---|---|
| | 8 June 1994 | Ph.D. Dissertation |

**4. TITLE AND SUBTITLE**

The Modal Decomposition of an Impedance Tube

**5. FUNDING NUMBERS**

**6. AUTHOR(S)**

A. J. Hull

**7. PERFORMING ORGANIZATION NAME(S) AND ADDRESS(ES)**

Naval Undersea Warfare Center
Detachment New London
New London, Connecticut 06320

**8. PERFORMING ORGANIZATION REPORT NUMBER**

TR 10,675

**9. SPONSORING/MONITORING AGENCY NAME(S) AND ADDRESS(ES)**

**10. SPONSORING/MONITORING AGENCY REPORT NUMBER**

**11. SUPPLEMENTARY NOTES**

**12a. DISTRIBUTION/AVAILABILITY STATEMENT**

Approved for public release; distribution is unlimited.

**12b. DISTRIBUTION CODE**

**13. ABSTRACT (Maximum 200 words)**

Impedance tubes are commonly used for determining the acoustic impedance of a material. This process is accomplished by placing the material into the end of the tube, where it is subjected to acoustic energy. Additional uses for impedance tubes include the testing and calibration of microphones or instruments at a predetermined location inside the tube through insonification. Impedance tubes usually consist of long ducts, with a speaker mounted at one end or in the duct wall and with the material placed at the other end. Holes are drilled in the tube at various locations to allow pressure measurements with microphones. In the past, a steady-state continuous model was used to predict the response of an impedance tube for pressure excitation at one end and an unknown acoustic impedance at the other end. The work presented here extends the modeling of impedance tubes by developing an eigenvalue-based model of the tube in modal space that can incorporate the transient or steady-state response of velocity sources on the spatial domain and the pressure sources at the end of the tube. Experimental verification is included for several different test configurations. Finally, the inverse problem is solved, which allows the determination of acoustic impedance from the eigenvalues of the measured system response

**14. SUBJECT TERMS**

Acoustic Energy, Acoustic Impedance, Eigenvalue-Based Model, Impedance Tube, Inverse Problem, Modal Space, Pressure Excitation, Pressure Measurements

**15. NUMBER OF PAGES**

40

**16. PRICE CODE**

| 17. SECURITY CLASSIFICATION OF REPORT | 18. SECURITY CLASSIFICATION OF THIS PAGE | 19. SECURITY CLASSIFICATION OF ABSTRACT | 20. LIMITATION OF ABSTRACT |
|---|---|---|---|
| UNCLASSIFIED | UNCLASSIFIED | UNCLASSIFIED | SAR |

## TABLE OF CONTENTS

# LIST OF ILLUSTRATIONS

# LIST OF TABLES

# THE MODAL DECOMPOSITION OF AN IMPEDANCE TUBE

## 1. INTRODUCTION

The dynamic response of an enclosed acoustic system is determined by both the governing differential equations and associated boundary conditions. The problem was first addressed as early as 1878 by Raleigh when he modeled one-dimensional acoustic response. More current research has treated the response of hard-walled ducts with idealized reflecting and/or nonreflecting terminations to point source excitation (Snowdon, 1971; Doak, 1973a; Swinbanks, 1973; Trinder and Nelson, 1983; Tichy et al., 1984).

Ducts with idealized totally reflective boundary conditions result in self-adjoint differential operators that yield a standing wave model with mutually orthogonal modes. However, models of ducts with totally absorbent (nonreflecting) boundary conditions do not resonate, and wave propagation models are frequently used. Actual acoustic systems have nonidealized, partially reflective boundary conditions, yielding some combination of propagating and standing wave components in their acoustic pressure response (Davis et al., 1954; Spiekermann and Radcliffe, 1988a, 1988b).

The available analytical techniques, however, do not provide for the possibility that the acoustic response could be a combination of standing and propagating waves, nor do they consider the effect of partially absorptive boundary conditions on duct models. The partially absorptive boundary condition produces a nonself-adjoint differential operator. Thus, traditional methods of orthogonal mode shape discretization for this class of problems cannot be applied because the eigenfunctions are not orthogonal with the conventional inner product over the domain of the operator, and the conventional eigenfunction inner product does not decouple the state equations of the model.

This paper develops an infinite order, diagonal, state-space model of a duct with a partially absorptive boundary condition by deriving a new method to orthogonalize the state equations. Mathematically, the model of duct pressure at some location in the spatial domain divided by the forcing function is a complex transfer function obtained by manipulating the nonself-adjoint differential operator of the system. The model is experimentally verified for several different test configurations. As described at the end of this paper, the model also provides a method for evaluating duct endpoint impedances based on the system eigenvalues.

## 2. SYSTEM MODEL

The system model is a one-dimensional, hard-walled duct excited by either a pressure input at one end or a particle velocity input into the spatial domain. The boundary conditions are a pressure release boundary condition at one end and a generalized impedance boundary condition at the other. This partially reflective boundary allows the acoustic response model to include standing and propagating wave responses simultaneously. This occurs when of some energy in the duct is dissipated out the end, while the remainder is reflected back into the duct.

The forced linear second-order wave equation for modeling particle displacement in a one-dimensional hard-walled duct is (Seto, 1971; Doak, 1973b; Morse and Ingard, 1968)

$$\frac{\partial^2 u(x,t)}{\partial t^2} - c^2 \frac{\partial^2 u(x,t)}{\partial x^2} = \frac{P(t)\delta(x)}{\rho} + \frac{\partial V(t)}{\partial t} R(x - x_s) , \qquad (1)$$

where $u(x,t)$ is the particle displacement (m), $c$ is the acoustic wave speed (m/s), $x$ is the spatial location (m), $t$ is time (s), $\rho$ is the density of the medium (kg/m$^3$), $P(t)$ is the pressure excitation at $x = 0$ (N/m$^2$), $V(t)$ is the particle velocity excitation at $x = x_s$ (m/s), $\delta(x)$ is the Dirac delta function (1/m), and $R(x - x_s)$ is the rectangular function (dimensionless). The rectangular function is defined as unity (1) for $x = 0$ to $x = x_s$ and as zero (0) everywhere else. The left-hand side of equation (1) represents the dynamics of the duct and the right-hand side represents the forcing functions acting on the duct. The wave

equation assumes an adiabatic system, no mean flow in the duct, a uniform duct cross section, and negligible air viscosity effects. The hard-wall assumption models the duct as having no dissipation on the domain. The one-dimensional assumption requires the diameter of the duct to be small compared with its length, which is valid when $f < 0.586(c/d)$, where $f$ is the frequency (Hz) and $d$ is the diameter of the duct (m) (Annual Book of ASTM Standards, 1985a, 1985b)

The boundary condition at the location $x = L$ is a generalized condition that corresponds to the acoustic impedance at the end of the duct. It is expressed as the relationship between the spatial gradient and the time gradient of particle displacement (Seto, 1971; Pierce, 1981) as follows:

$$\frac{\partial u(L,t)}{\partial x} = -K\left(\frac{1}{c}\right)\frac{\partial u(L,t)}{\partial t} , \tag{2}$$

where $K$ is the acoustic impedance of the termination end (dimensionless). For a steady-state response in the duct, $K$ can be a complex number. For a transient response, $K$ is a real number. Implicit in equation (2) is the analogy with electrical systems, where acoustic velocity corresponds to current and duct pressure to voltage. When $\text{Re}(K)$ equals zero or infinity, the termination end of the duct reflects all the acoustic energy, and the response is composed of standing waves only. When $K = 1 + 0i$, the termination end of the duct absorbs all the acoustic energy, and the response is composed of propagating waves. All other values of $K$ yield some mixed combination of propagating and standing wave response. In general, the reflection coefficient $(1 - K)/(1 + K)$ gives the relative magnitude of the reflected pressure wave off the termination end. The real part of $K$ (acoustic resistance) is associated with energy dissipation and is sometimes called a loss coefficient because it is a measure of the amount of energy leaving the duct. The imaginary part of $K$ (acoustic reactance) is associated with conservative fluid compliance and/or inertia effects.

The duct end at $x = 0$ is modeled as a pressure release boundary condition:

$$\frac{\partial u(0,t)}{\partial x} = 0 \; . \tag{3}$$

At low frequencies, this equation corresponds to an open duct end or one with an excitation speaker. The acoustic pressure of the system is related to the spatial gradient of the particle displacement by (Seto, 1971)

$$P(x,t) = -\rho c^2 \frac{\partial u(x,t)}{\partial x} \; . \tag{4}$$

Equations (1)-(4) represent a mathematical model of the duct for one-dimensional motion. An impedance tube with two excitation sources is shown in Figure 1, although only one source is typically used for an experiment.
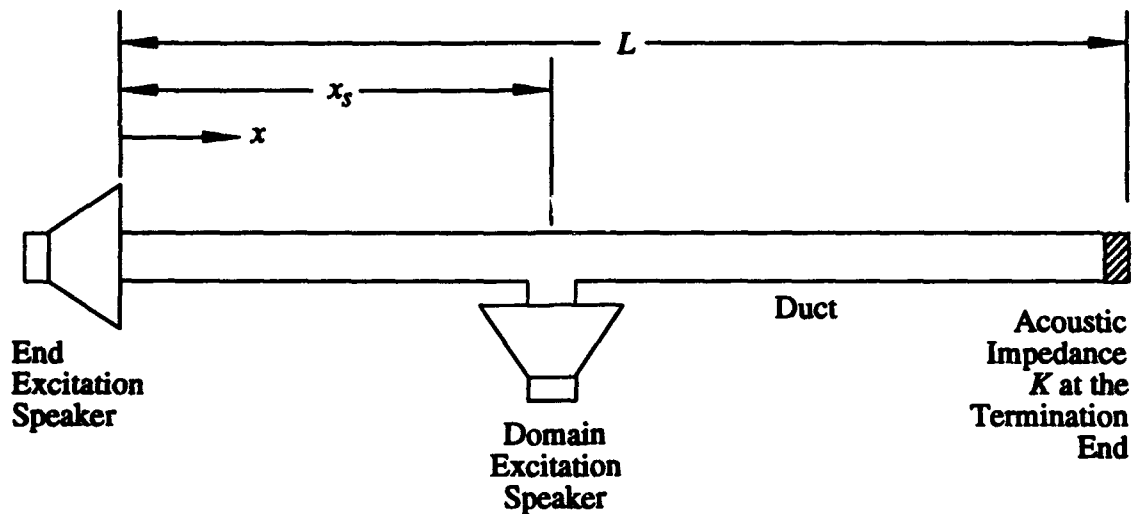


Figure 1. A Typical Impedance Tube With Excitation Sources

4

## 3. A DECOUPLED SOLUTION

A decoupled set of ordinary differential equations in state-space form that model the dynamic response is now developed. These equations will incorporate the boundary conditions (equations (2) and (3)) as well as the initial conditions in the duct. The eigenvalues and eigenfunctions of the model are found by applying separation of variables to equations (2) and (3) and to the homogeneous version of equation (1).

Separation of variables assumes that each term of the solution is a product of a function in the spatial domain multiplied by a function in the time domain:

$$u(x,t) = X(x)T(t) . \tag{5}$$

Substituting equation (5) into the homogeneous version of equation (1) produces two independent ordinary differential equations, each with complex-valued separation constant $\lambda$ ; namely,

$$\frac{d^2 X(x)}{dx^2} - \lambda^2 X(x) = 0 \tag{6}$$

and

$$\frac{d^2 T(t)}{dt^2} - c^2 \lambda^2 T(t) = 0 . \tag{7}$$

The separation constant $\lambda = 0$ is a special case, where $X(x) = T(t) =$ a constant to satisfy equations (2) and (3). Because the pressure field is proportional to the spatial derivative of the particle displacement, the separation constant $\lambda = 0$ (and its associated particle displacement term) will not contribute to the pressure field. The spatial ordinary differential equation (equation (6)) is solved for $\lambda \neq 0$ with the boundary condition given in equation (3):

$$X(x) = e^{\lambda x} + e^{-\lambda x} . \tag{8}$$

The time-dependent ordinary differential equation (equation (7)) yields the following general solution:

$$T(t) = Ae^{c\lambda t} + Be^{-c\lambda t} \ .$$ (9)

Applying the boundary condition of equation (2) to equations (8) and (9) results in $B = 0$ and the integer-indexed separation constants

$$\lambda_n = \frac{1}{2L}\log_e\left(\frac{1-K}{1+K}\right) - \frac{n\pi i}{L} \ , \qquad n = \ ...-3,-2,-1, \ 0, \ 1, \ 2, \ 3,... \ \ ,$$ (10)

where $i$ is equal to the square root of $-1$ and $\lambda$ has units of inverse meters. Inserting the indexed separation constants into equation (8) produces the complex-valued spatial eigenfunctions

$$\varphi_n(x) = e^{\lambda_n x} + e^{-\lambda_n x} \ .$$ (11)

The eigenvalues of the system are equal to the separation constant multiplied by the wave speed as follows:

$$\Lambda_n = c\lambda_n \ ,$$ (12)

where $\Lambda_n$ has units of radians/second. A plot of the eigenvalues in the complex plane is shown in Figure 2. The indexed eigenvalues are equally spaced and parallel to the imaginary axis. The $n = 2$ eigenfunction is shown in Figure 3 for acoustic impedances of $K = 0.5 + 0i$ and $K = 0 + 0i$. Unless the acoustic impedance $K$ is zero or infinity, the eigenfunctions are not mutually orthogonal on $[0,L]$, conventional modal analysis of the forced wave equation is not possible, and the time response cannot be found.

Figure 2.  System Eigenvalues $\Lambda_n$ for Constant $K$

The following expressions appear as axis labels in the figure:

$$\left[\frac{c}{2L}\arg\left(\frac{1-K}{1+K}\right)+\frac{3c\pi}{L}\right]i$$

$$\left[\frac{c}{2L}\arg\left(\frac{1-K}{1+K}\right)+\frac{2c\pi}{L}\right]i$$

$$\left[\frac{c}{2L}\arg\left(\frac{1-K}{1+K}\right)+\frac{c\pi}{L}\right]i$$

$$\left[\frac{c}{2L}\arg\left(\frac{1-K}{1+K}\right)\right]i$$

$$\frac{c}{2L}\log_e\left|\frac{1-K}{1+K}\right|$$

$$\left[\frac{c}{2L}\arg\left(\frac{1-K}{1+K}\right)-\frac{c\pi}{L}\right]i$$

$$\left[\frac{c}{2L}\arg\left(\frac{1-K}{1+K}\right)-\frac{2c\pi}{L}\right]i$$

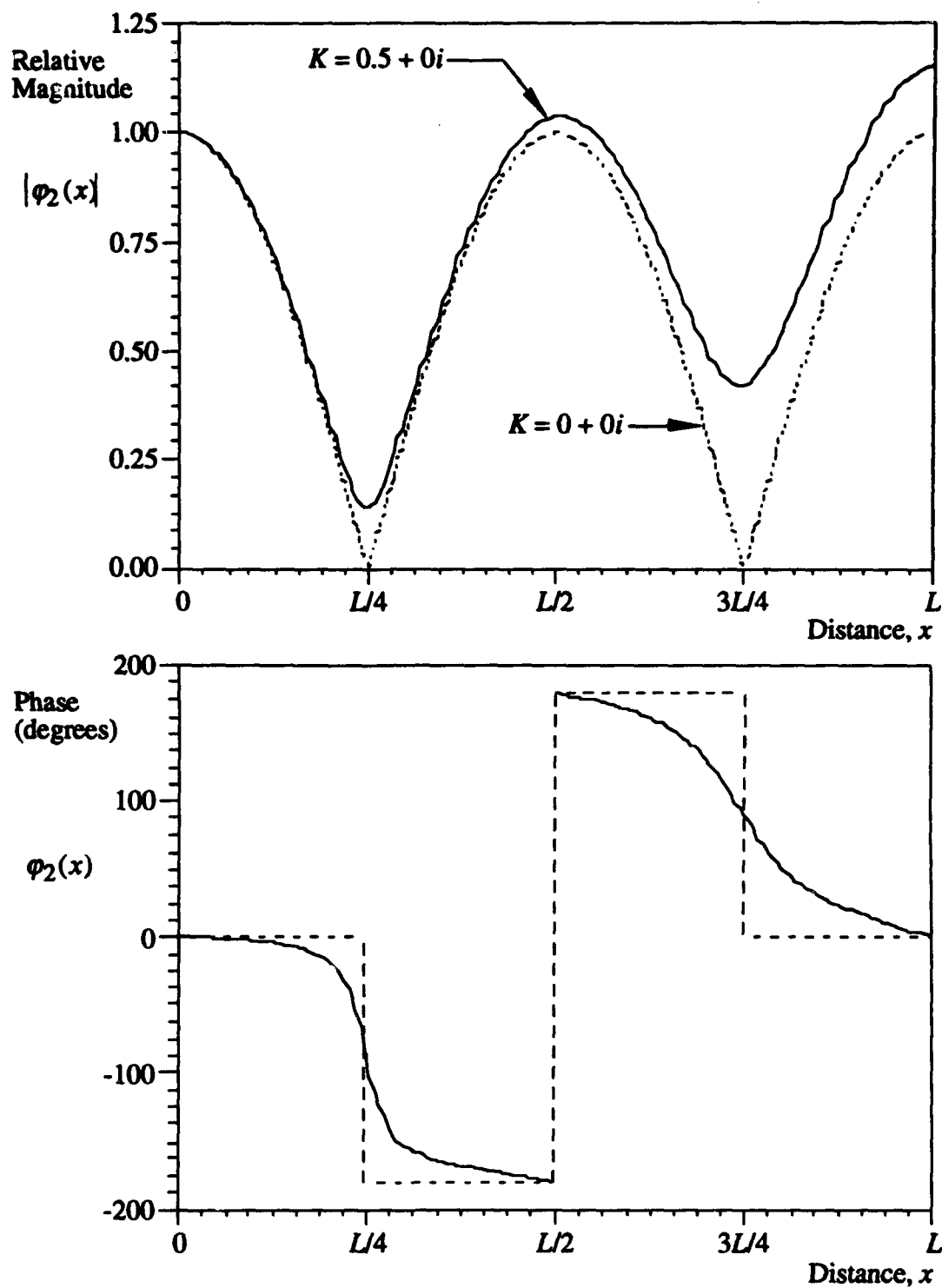$$\left[\frac{c}{2L}\arg\left(\frac{1-K}{1+K}\right)-\frac{3c\pi}{L}\right]i$$

Figure 3. Second Eigenfunction With End Impedances of $K = 0.5 + 0i$ and $K = 0 + 0i$

As discussed earlier, traditional methods of orthogonal mode shapes cannot be applied here because of the nonself-adjoint operator. However, by extending the problem definition onto a virtual duct and then redefining the equations over $[-L,L]$, the time and space modes will decouple and a solution to the problem can be found. This technique is explained next.

The particle displacement (or solution) to the forced wave equation is now written as a series solution plus a time-dependent term arising from the $\lambda = 0$ separation constant. This expression is

$$u(x,t) = G(t) + \sum_{n=-\infty}^{\infty} a_n(t)\, \varphi_n(x) \,, \tag{13}$$

where $G(t)$ and $a_n(t)$ are generalized coordinates (state variables) and $\varphi_n(x)$ represents the spatial eigenfunctions defined in equation (11). The coordinate $G(t)$ will not contribute to the pressure response in the duct because the pressure response is only dependent on the spatial partial derivative. Derivation of a solution that decouples the time and space modes requires the time derivative (velocity) of the particle displacement to be written in two different forms. The first form is the time derivative of equation (13) and yields

$$\frac{\partial u(x,t)}{\partial t} = \frac{dG(t)}{dt} + \sum_{n=-\infty}^{\infty} \frac{da_n(t)}{dt}\, \varphi_n(x) \,. \tag{14}$$

The second, developed by using equations (5), (9), and (12), is written as

$$\frac{\partial u(x,t)}{\partial t} = \sum_{n=-\infty}^{\infty} \Lambda_n\, a_n(t)\, \varphi_n(x) \,. \tag{15}$$

Equating equations (14) and (15) produces

$$\frac{dG(t)}{dt} + \sum_{n=-\infty}^{\infty} \left[ \frac{da_n(t)}{dt} - \Lambda_n a_n(t) \right] \varphi_n(x) = 0 \,. \tag{16}$$

The assumption is now made that differentiation will distribute over the summation, which will be validated by decoupled space and time modes. The forced wave equation (equation (1)) is rewritten with the equations (13)-(16). The second partial time derivative is found

from the time derivative of equation (15), and the second partial spatial derivative is found from the second spatial derivative of equation (13). Inserting these derivatives into the left-hand side of equation (1) yields

$$\sum_{n=-\infty}^{\infty} \left[ \frac{da_n(t)}{dt} - \Lambda_n a_n(t) \right] \Lambda_n \varphi_n = \frac{P(t)\delta(x)}{\rho} + \frac{\partial V(t)}{\partial t} R(x - x_s) \; . \tag{17}$$

Equation (16) is now differentiated with respect to $x$ and multiplied by the wave speed $c$. The result is then added to equation (17) to form

$$\sum_{n=-\infty}^{\infty} \left[ \frac{da_n(t)}{dt} - \Lambda_n a_n(t) \right] \Lambda_n 2 e^{\lambda_n x} = \frac{P(t)\delta(x)}{\rho} + \frac{\partial V(t)}{\partial t} R(x - x_s) \; , \qquad x \in [0,L] \; , \tag{18}$$

and is subtracted from equation (17) to give

$$\sum_{n=-\infty}^{\infty} \left[ \frac{da_n(t)}{dt} - \Lambda_n a_n(t) \right] \Lambda_n 2 e^{-\lambda_n x} = \frac{P(t)\delta(x)}{\rho} + \frac{\partial V(t)}{\partial t} R(x - x_s) \; , \qquad x \in [0,L] \; . \tag{19}$$

The interval of equation (19) is changed from [0,L] to [-L,0] by substitution of $-x$ for $x$, producing

$$\sum_{n=-\infty}^{\infty} \left[ \frac{da_n(t)}{dt} - \Lambda_n a_n(t) \right] \Lambda_n 2 e^{\lambda_n x} = \frac{P(t)\delta(-x)}{\rho} + \frac{\partial V(t)}{\partial t} R(-x - x_s) \; , \qquad x \in [-L,0] \; . \tag{20}$$

Combining equations (18) and (20) into a single equation and breaking the exponential into terms that contain the index $n$ and terms that do not contain the index $n$ results in

$$\sum_{n=-\infty}^{\infty} \left[ \frac{da_n(t)}{dt} - \Lambda_n a_n(t) \right] 2 \Lambda_n e^{\frac{-in\pi x}{L}} =$$

$$\begin{cases} e^{\frac{-1}{2L}\log_e\left(\frac{1-K}{1+K}\right)x} \left[ \dfrac{P(t)\delta(-x)}{\rho} + \dfrac{\partial V(t)}{\partial t} R(-x - x_s) \right] , & x \in [-L,0] \; , \\[4em] e^{\frac{-1}{2L}\log_e\left(\frac{1-K}{1+K}\right)x} \left[ \dfrac{P(t)\delta(x)}{\rho} + \dfrac{\partial V(t)}{\partial t} R(x - x_s) \right] , & x \in [0,L] \; . \end{cases} \tag{21}$$

10

The exponential function $e^{im\pi x/L}$ (where $m$ is an integer) is now multiplied on both sides of equation (21), and the resulting equation is integrated from $-L$ to $L$. The left-hand side of the equation can be expressed as

$$\int_{-L}^{L}\left[\frac{da_n(t)}{dt}-\Lambda_n a_n(t)\right]2\Lambda_n e^{\frac{-in\pi x}{L}}e^{\frac{im\pi x}{L}}dx =$$

$$\begin{cases}\left[\dfrac{da_n(t)}{dt}-\Lambda_n a_n(t)\right]4\Lambda_n L \quad , \quad n=m, \\[4mm] 0 \quad , \hspace{3.5cm} n\neq m. \end{cases} \tag{22}$$

Use of the reflection property of integrals and the bound of $0 < x_s < L$ results in the right-hand side of equation (21) becoming

$$\int_{-L}^{0}e^{-\lambda_n x}\left[\frac{P(t)\delta(-x)}{\rho}+\frac{\partial V(t)}{\partial t}R(-x-x_s)\right]dx \quad +$$

$$\int_{0}^{L}e^{-\lambda_n x}\left[\frac{P(t)\delta(x)}{\rho}+\frac{\partial V(t)}{\partial t}R(x-x_s)\right]dx \quad =$$

$$\frac{2P(t)}{\rho} \quad + \quad \frac{1}{\lambda_n^2}\frac{d\varphi_n(x_s)}{dx}\frac{\partial V(t)}{\partial t} . \tag{23}$$

Equations (22) and (23) can be equated (for $n = m$) to form ordinary differential equations for the generalized coordinates $a_n$ as

$$\frac{da_n(t)}{dt}-\Lambda_n a_n(t) = \frac{P(t)}{2\Lambda_n L\rho} + \frac{1}{4\Lambda_n L\lambda_n^2}\frac{d\varphi_n(x_s)}{dx}\frac{\partial V(t)}{\partial t} . \tag{24}$$

An explicit solution to equation (24) cannot be found until a time-dependent forcing function has been specified.

The initial conditions of the generalized coordinates can be determined from the initial conditions of the duct with a method similar to the above derivation. This equation is

$$a_n(0) = \frac{1}{4\Lambda_n L} \int\limits_0^L \frac{\partial u(x,0)}{\partial t} \varphi_n(x) dx + \frac{1}{4\lambda_n^2 L} \int\limits_0^L \frac{\partial u(x,0)}{\partial x} \frac{d\varphi_n(x)}{dx} dx , \qquad (25)$$

where $\partial u(x,0)/\partial t$ is the initial velocity of the acoustic medium (m/s) and $\partial u(x,0)/\partial x$ is the initial acoustic strain in the duct (dimensionless), which is proportional to initial pressure (equation (4)).

## 4. ACCURACY OF TRUNCATED SOLUTION

The exact series solution must be truncated to a finite number of terms. The effect of this truncation on steady-state pressure excitation (at $x = 0$) will now be examined since a closed-form solution already exists for this case. The exact steady-state series solution for pressure excitation at $x = 0$ is found by solving equation (24) using $P(t) = P_0 e^{i\omega t}$ (where $\omega$ = frequency in radians/second) and $V(t) = 0$ and then inserting the resulting generalized coordinates $a_n(t)$ into equation (4). The transfer function between pressure in the domain $P(x,t)$ and the amplitude of the excitation $P_0$ is

$$\frac{P(x,t)}{P_0} = \frac{-c}{2L} \left[ \sum_{n=-\infty}^{\infty} \frac{e^{\lambda_n x} - e^{-\lambda_n x}}{(i\omega - \Lambda_n)} \right] e^{i\omega t} , \qquad (26)$$

which is truncated to a $2N + 1$ term series by

$$\frac{P(x,t)}{P_0} = \frac{-c}{2L} \left[ \sum_{n=-N}^{N} \frac{e^{\lambda_n x} - e^{-\lambda_n x}}{(i\omega - \Lambda_n)} \right] e^{i\omega t} . \qquad (27)$$

The exact steady-state response for the system described in equations (1)-(4) has been independently calculated (Spiekermann and Radcliffe, 1988a) for harmonic pressure excitation at $x = 0$ in continuous closed-form solution as

$$\frac{P(x,t)}{P_0} = \left[ \frac{(K+1)e^{i\frac{\omega}{c}(L-x)} + (K-1)e^{-i\frac{\omega}{c}(L-x)}}{(K+1)e^{i\frac{\omega}{c}L} + (K-1)e^{-i\frac{\omega}{c}L}} \right] e^{i\omega t} . \qquad (28)$$

This exact steady-state response model is only valid for the special case of harmonic pressure excitation at $x = 0$. It cannot model the velocity excitation in the domain, nor can

12

it model transient responses. It is used here only for comparison with the more general result of equation (26).

Quantitative information on the accuracy of a truncated, steady-state, series solution (equation (27)) is found here by comparing it to an exact, steady-state frequency response (equation (28)). Figure 4 shows the frequency response of a 1.524-m (5-ft) duct at a location of $x = 0.4267$ m (1.4 ft) from pressure excitation at $x = 0$. The impedance at $x = L$ is $K = 0.3 + 0.2i$, and a truncated series model with 11 terms is used to approximate the exact solution. The solid line is the truncated steady-state series solution (equation (27)) and the dashed line is the continuous solution (equation (28)). The mean relative error up to the fifth duct resonance is only 3.2 percent (-30 dB). Numerical simulations suggest that the state-space model requires one state to model zero frequency response plus two states to model each duct resonance. The model yields acceptable accuracy up to the highest duct resonance modeled.
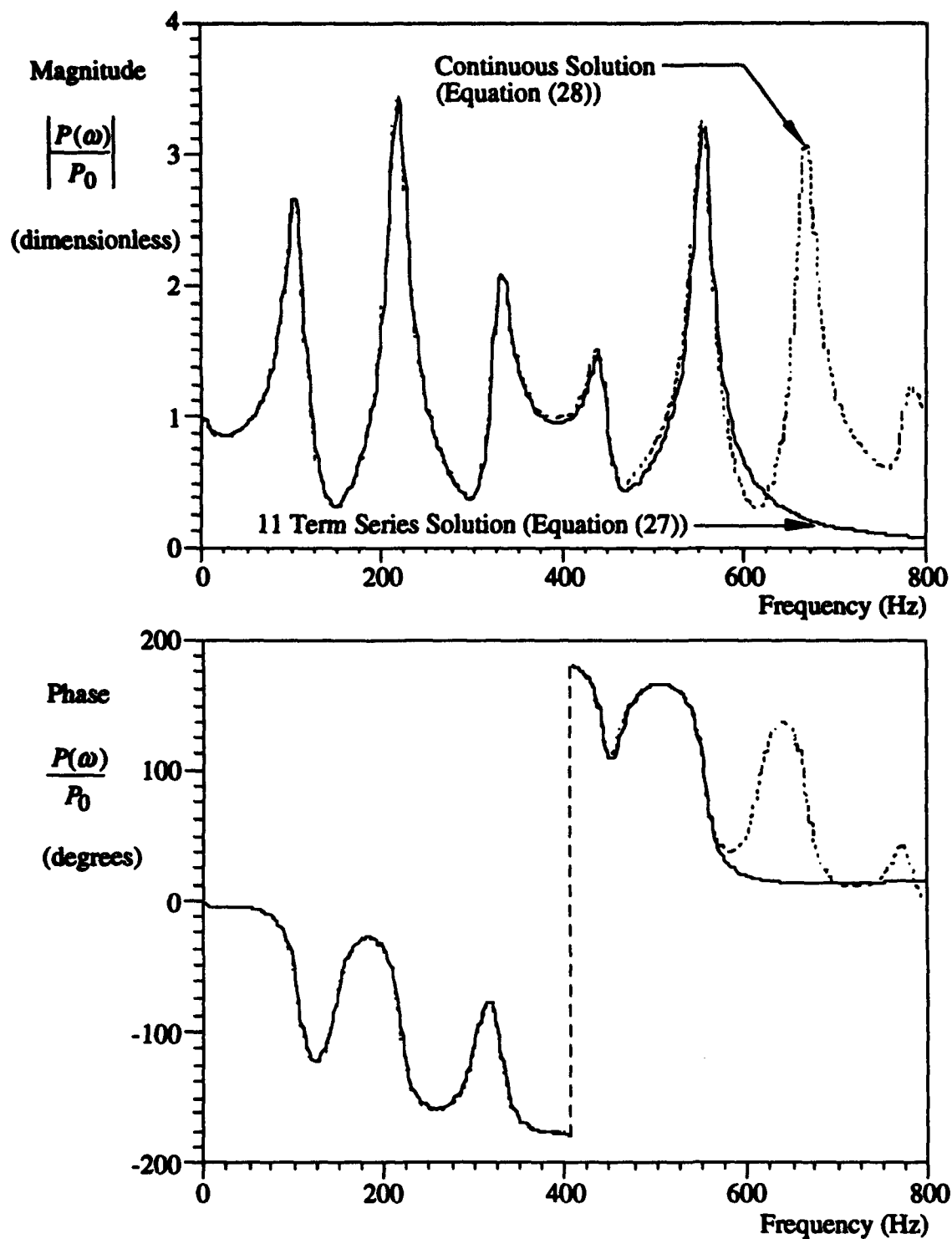
Figure 4. Theoretical Frequency Responses With Acoustic Impedance $K = 0.3 + 0.2i$

## 5. MODEL VALIDATION EXPERIMENTS

The state-space model developed above is experimentally verified for four different test cases: steady-state pressure excitation with frequency-invariant (constant) acoustic impedance, steady-state velocity excitation with frequency-invariant acoustic impedance, steady-state pressure excitation with frequency-dependent acoustic impedance, and transient pressure excitation with constant impedance. In all the experiments, the impedance at the end of the duct was calculated from the experimental system transfer functions. This impedance measurement technique is described next.

### 5.1. STEADY-STATE PRESSURE EXCITATION WITH FREQUENCY-INVARIANT ACOUSTIC IMPEDANCE

The first experiment involved steady-state pressure excitation at $x = 0$ with a constant, frequency-invariant acoustic impedance at the termination end. The impedance was produced by inserting a flat piece of packing foam that had a nearly constant impedance at all frequencies of interest (approximately $K = 0.285 + 0.079i$ from zero to 400 Hz). The theoretical response of the system is given by equation (27). The experiment used a 76-mm (3-in.) circular PVC schedule-40 duct that was 2.60 m (8.52 ft) long driven by a 254-mm (10-in.) diameter speaker (Realistic 40-1331B). Input pressure of the speaker was measured at its exit plane with a Bruel and Kjaer Type 4166 half-inch microphone attached to a Hewlett Packard 5423A digital signal analyzer. At a location of $x$ = 0.792 m (2.60 ft) from the speaker, the response of the tube was measured with another Bruel and Kjaer Type 4166 half-inch microphone. The output of the response measurement microphone was then connected to the signal analyzer (Figure 5). Both microphones were calibrated using a Bruel and Kjaer Type 4230 Sound Level Calibrator. The results of the experiment are shown in Figure 6. The measured responses are marked by X's and the theoretical response by a solid line. There is a high degree of accuracy in the magnitude and phase data. The disagreement between the experimental data and the theory is possibly due to a slight nonlinearity of the packing foam impedance.
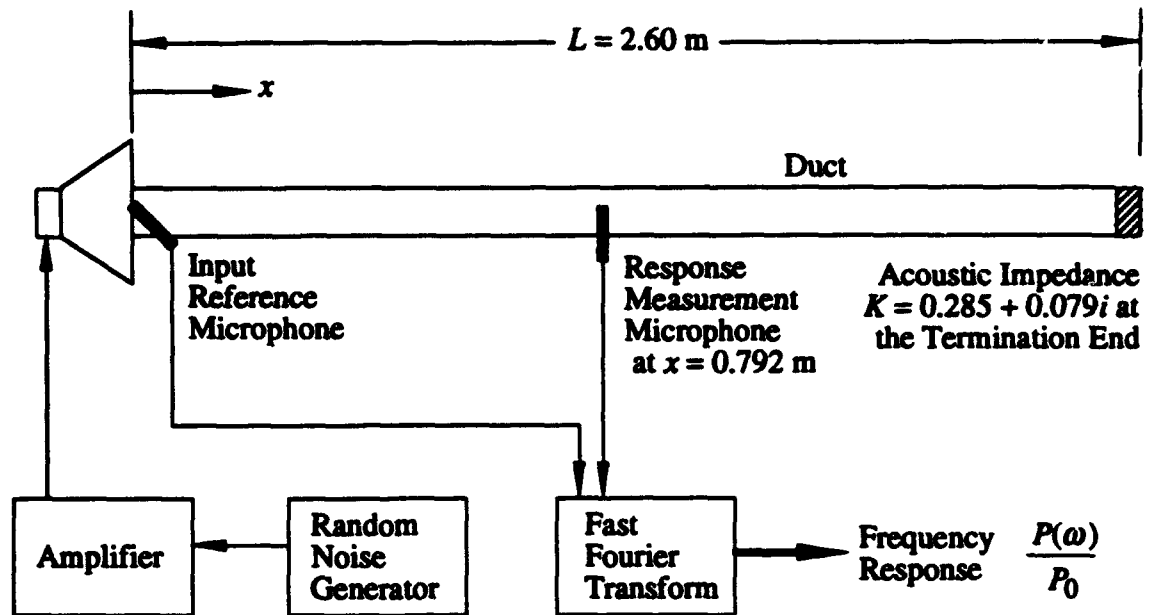
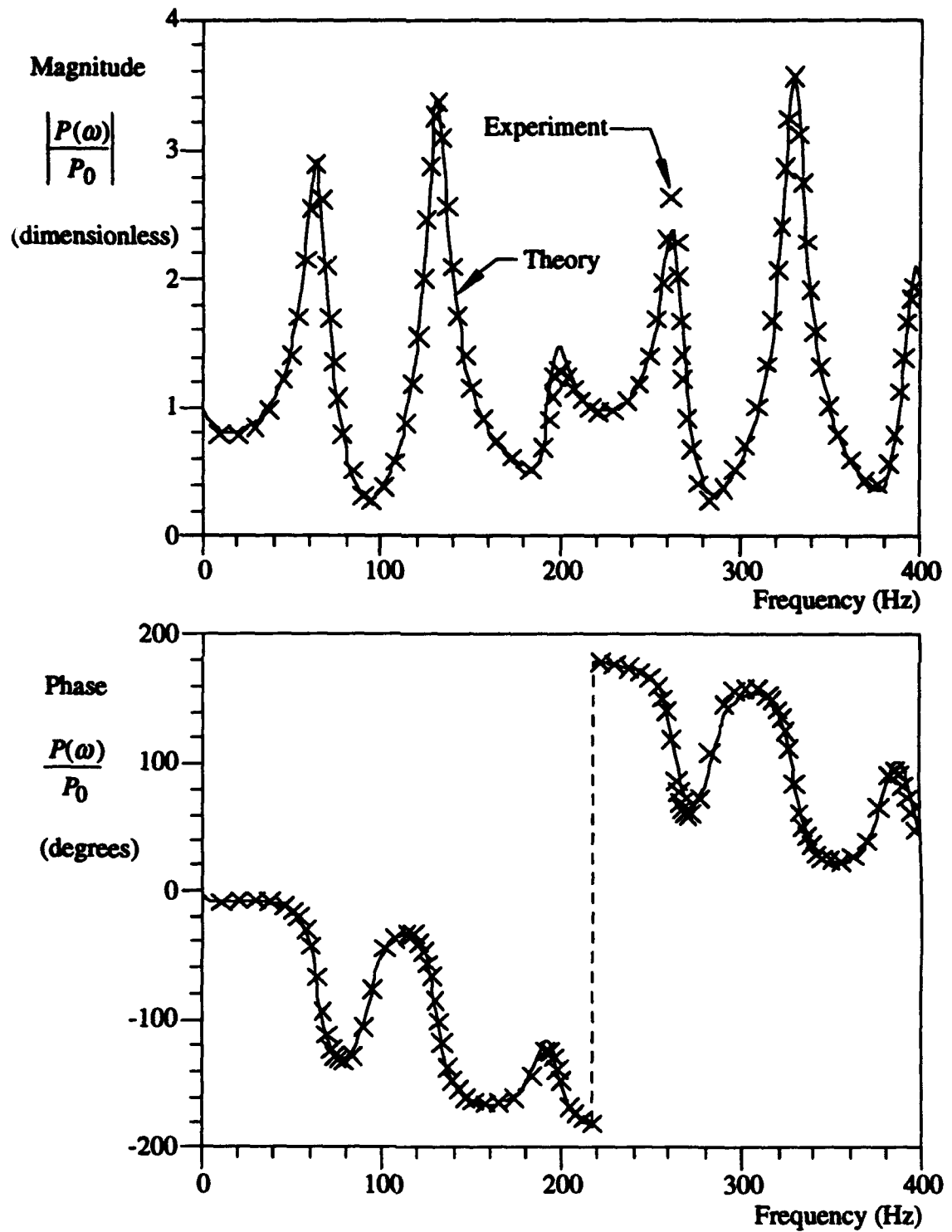Figure 5.  Laboratory Configuration for First Experiment

Figure 6. Theoretical and Experimental Frequency Responses for First Test

## 5.2. STEADY-STATE VELOCITY EXCITATION WITH FREQUENCY-INVARIANT ACOUSTIC IMPEDANCE

The experiment was rerun with velocity excitation in the domain. The truncated steady-state transfer function of the system with a velocity excitation of $V(t) = V_0 e^{i\omega t}$ at $x_s$ is

$$\frac{P(x,t)}{V_0} = \frac{-i\omega\rho c^2}{4L} \left[ \sum_{n=-N}^{N} \frac{(e^{\lambda_n x_s} - e^{-\lambda_n x_s})(e^{\lambda_n x} - e^{-\lambda_n x})}{(i\omega - \Lambda_n)\Lambda_n} \right] e^{i\omega t} . \qquad (29)$$

A Realistic 102-mm (4-in.) speaker was located in the wall of the duct at $x_s = 1.58$ m (5.17 ft) with a schedule-40 test tee. The input signal was measured with a Bruel and Kjaer Type 3544 helium neon laser velocity measurement system attached to the signal analyzer. The test tee had a Plexiglas window inserted in its side so that the laser could illuminate the speaker cone face in order to measure speaker velocity. The length of the duct tested was 4.42 m (14.5 ft), and the response was measured at $x = 0.762$ m (2.50 ft). The foam used in the first experiment was again used in this one. A diagram of the laboratory configuration is shown in Figure 7; the results of the experiment are shown in Figure 8. The solid line denotes the theory (equation (29)) and the X's show the experimental data.
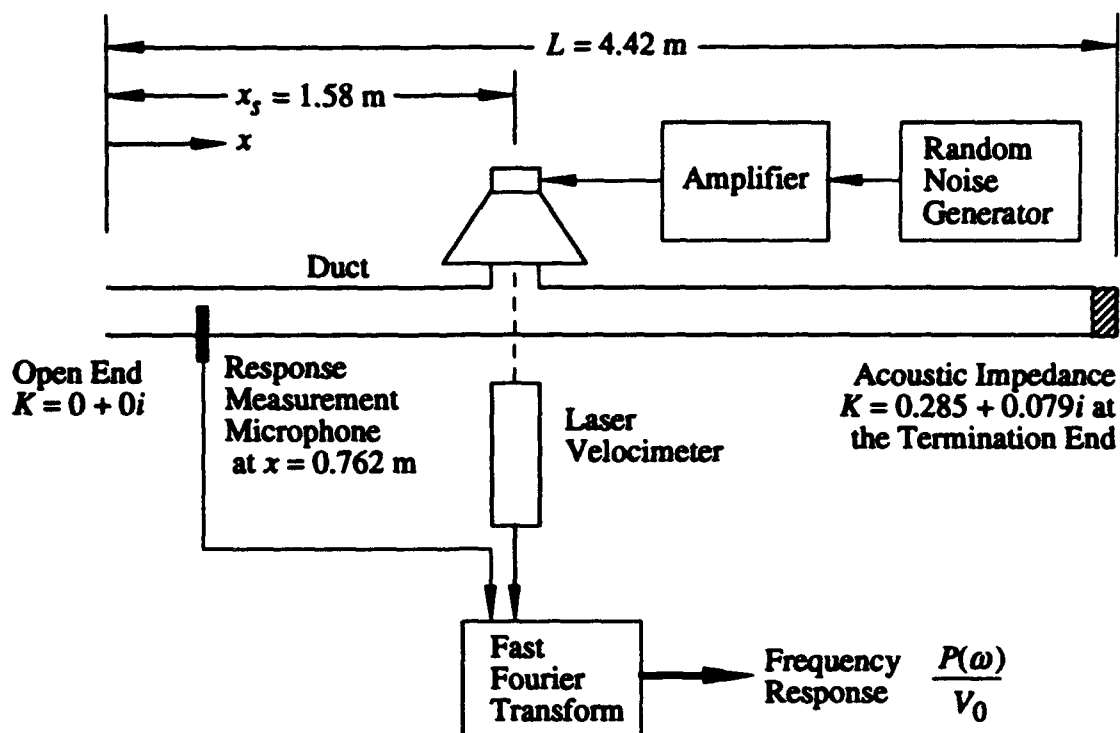
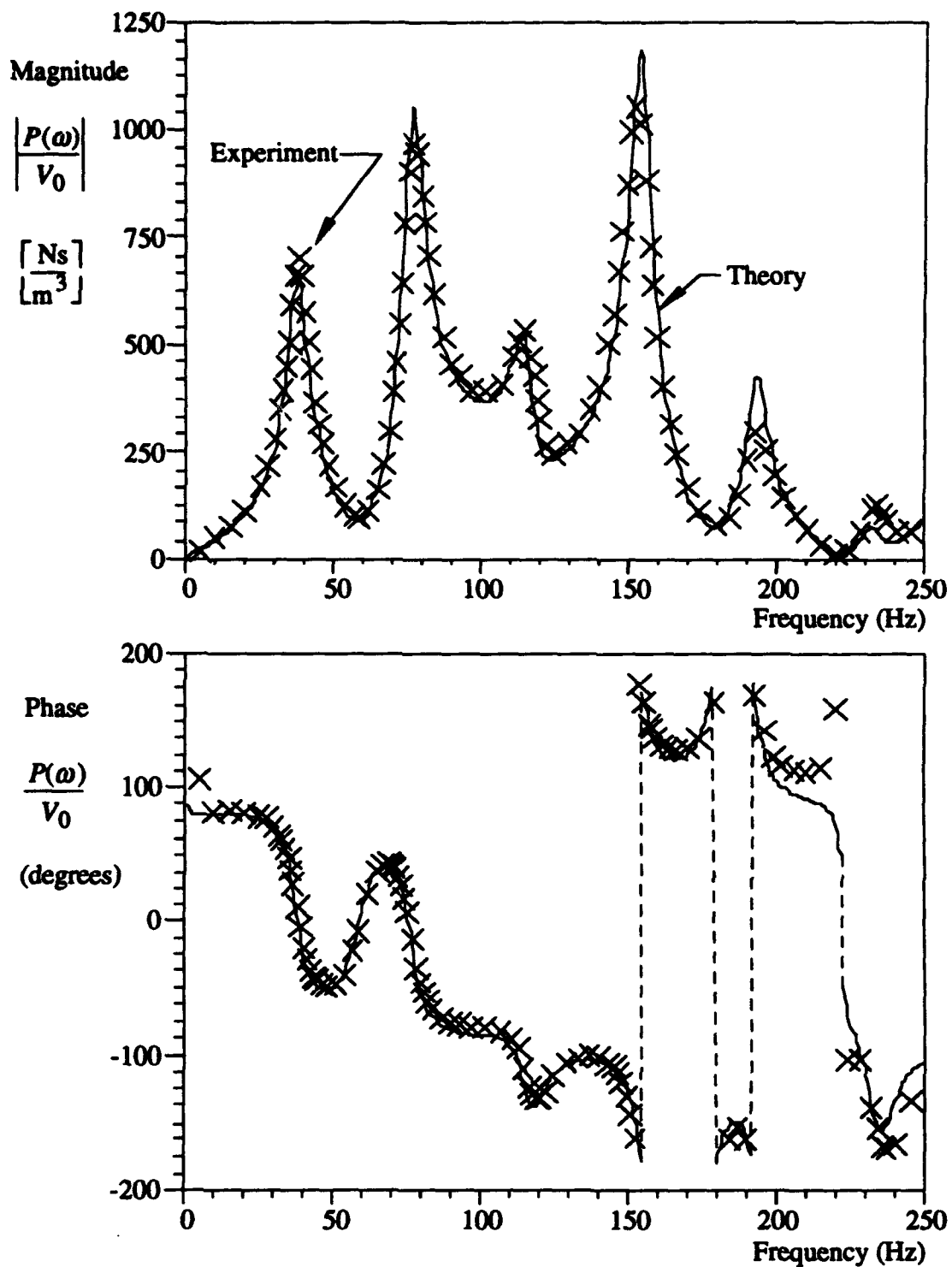Figure 7. Laboratory Configuration for Second Experiment

Figure 8. Theoretical and Experimental Frequency Responses for Second Test

## 5.3. STEADY-STATE PRESSURE EXCITATION WITH FREQUENCY-DEPENDENT ACOUSTIC IMPEDANCE

The acoustic impedance discussed here is given in equation (2), where it is assumed that acoustic impedance is frequency invariant. For some termination ends, the impedance is frequency dependent. For these systems, equation (2) is written as

$$\frac{\partial u(L,t)}{\partial x} = -K(\omega)\left(\frac{1}{c}\right)\frac{\partial u(L,t)}{\partial t} . \tag{30}$$

Although the separation of variables method is for a constant $K$, the termination ends where $K$ is a function of frequency can be approximated by the expression

$$\left.\frac{\partial u(L,t)}{\partial x}\right|_{\omega=\omega_n} \approx -K_n\left(\frac{1}{c}\right)\left.\frac{\partial u(L,t)}{\partial t}\right|_{\omega=\omega_n} . \tag{31}$$

With the relationship in equation (31), the state-space model derived above can be used to approximate systems with frequency-dependent terminations, as shown in the next experiment.

The third test involved pressure excitation at $x = 0$ with a nonconstant acoustic impedance in the termination end. The nonconstant termination was produced by placing a hemisphere of foam with a diameter equal to the duct diameter in the end of the duct at $x = L$. The resulting acoustic wave was affected by the presence and the shape of the material, which produced a nonconstant acoustic impedance. The impedance values listed in Table 1 were found by obtaining the frequency response of the system from zero to 800 Hz and then by solving the inverse problem for $K$ at each duct eigenvalue (described below). The length of the duct was 1.59 m (5.22 ft), and the response was measured at $x = 1.09$ m (3.56 ft). The experimental setup (with different physical dimensions) was the same one as shown in Figure 5. The state-space model was assembled with the individual acoustic impedance measurements of $K$ at each resonant frequency rather than at a single constant value. The eigenvalues of the system are nonconjugate complex values since $K$ is complex. A comparison of the theoretical transfer function and the experiment is shown in

Figure 9. This figure demonstrates that for a nonconstant impedance end the linear state-space model is reasonably accurate and can predict resonant peak locations as well as system phase angles. The errors tend to be minimized near the natural frequencies but maximized between them. This result occurred because the modal impedances $K_n$ were measured at the natural frequencies. The model does not account for varying values of the acoustic impedance between the modes.

Table 1. Calculated Acoustic Impedance.

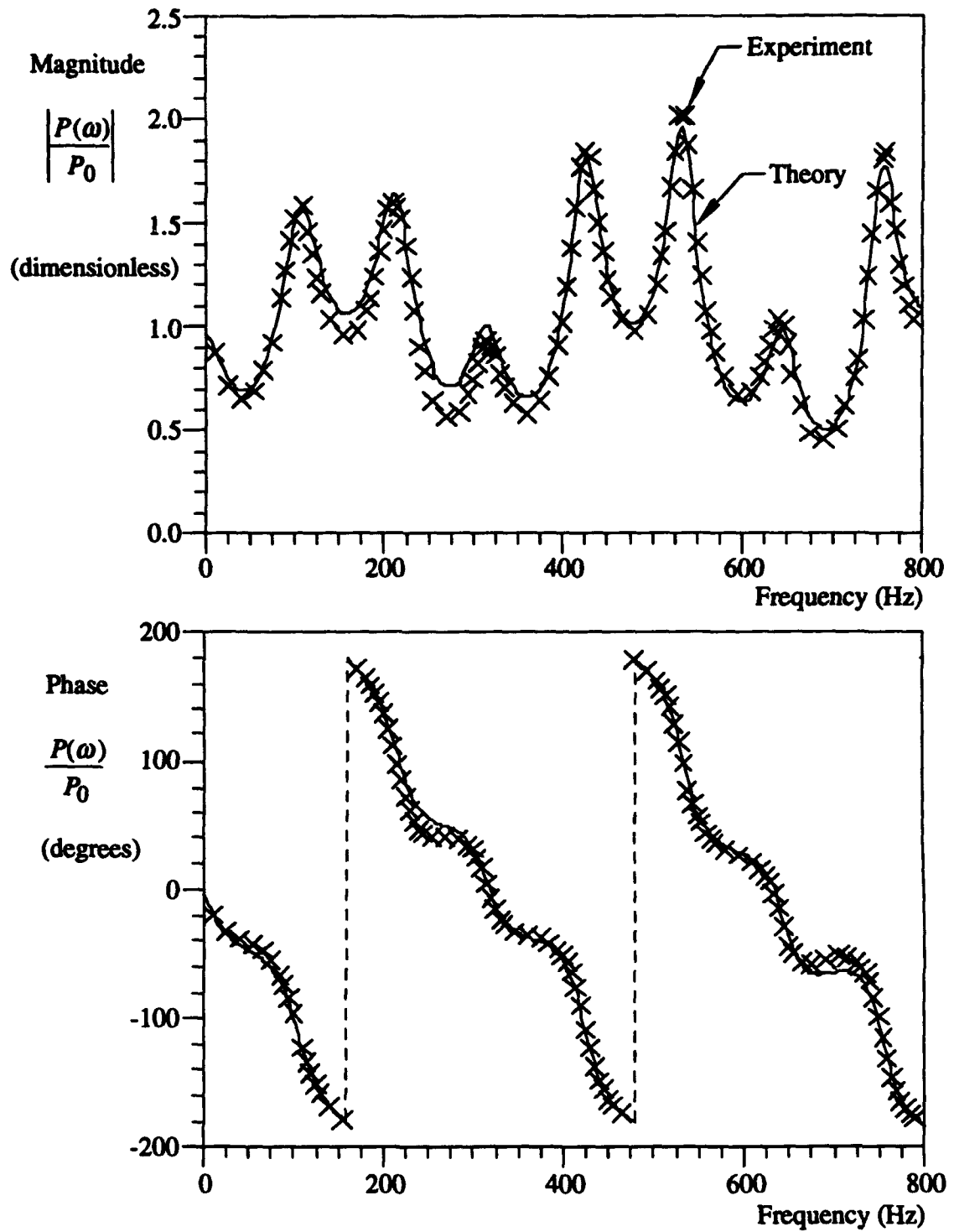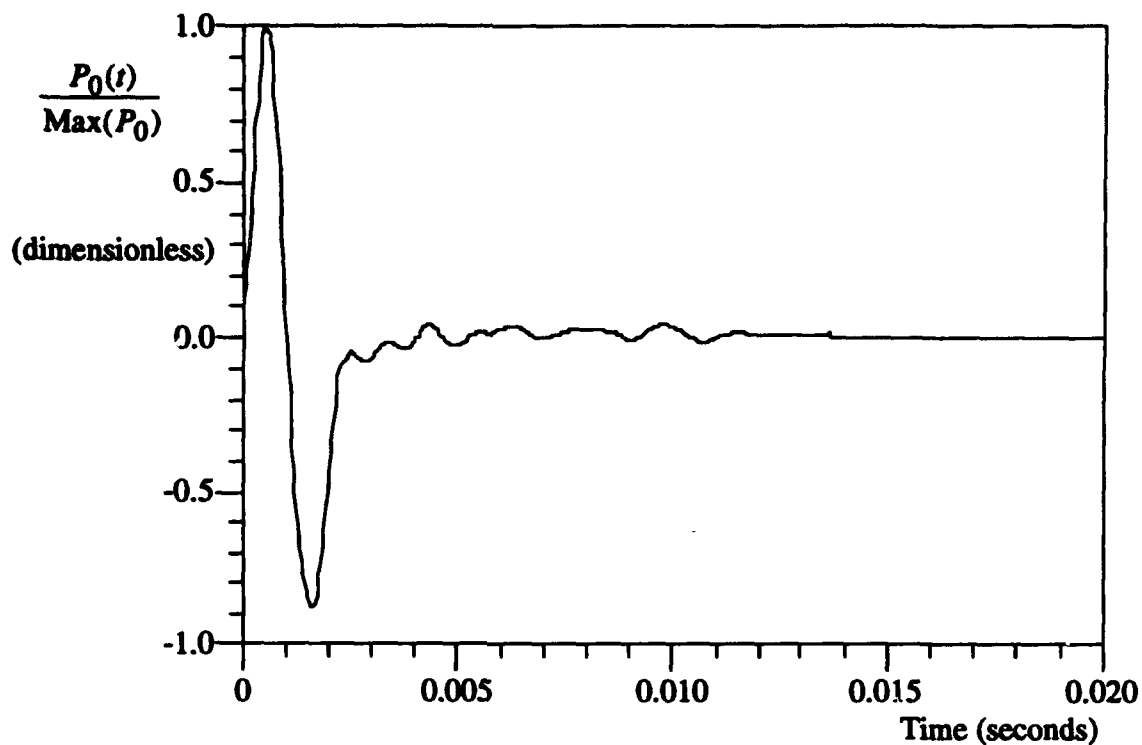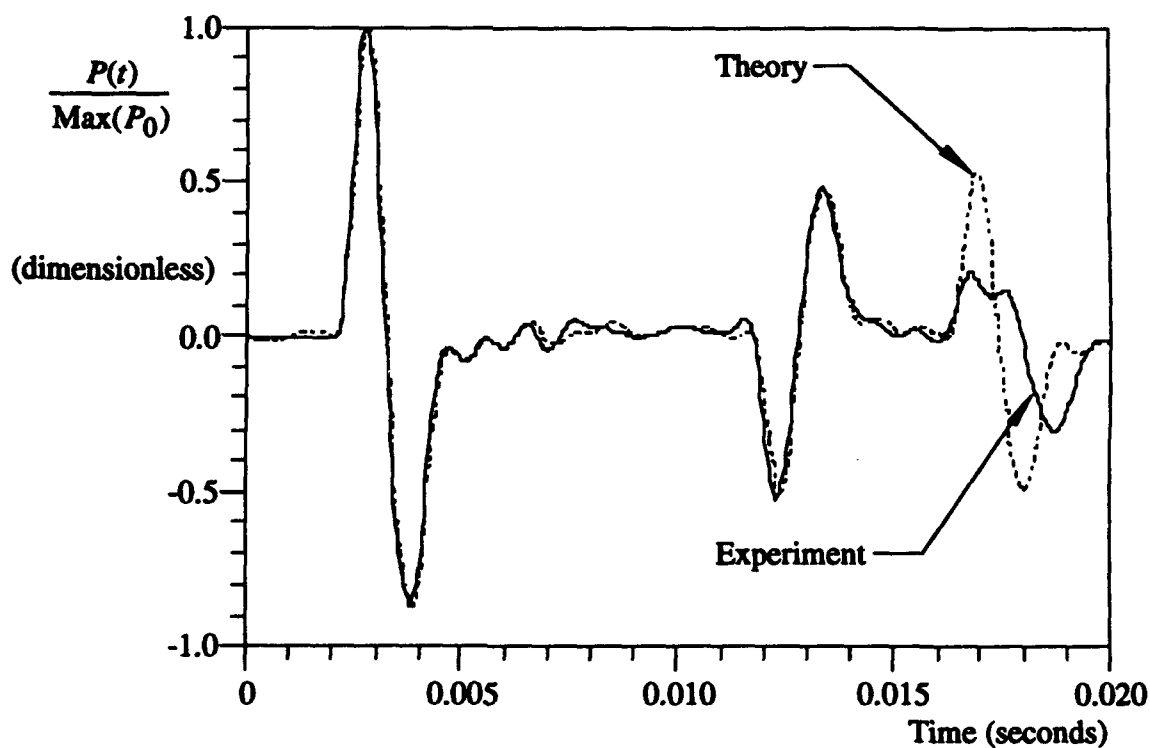| Eigenvalue ($n$) | $f_n$ (Hz) | Re ($K_n$) | Im ($K_n$) |
|:---:|:---:|:---:|:---:|
| 1 | 104.8 | 0.599 | 0.066 |
| 2 | 213.8 | 0.585 | 0.054 |
| 3 | 314.6 | 0.594 | 0.206 |
| 4 | 424.2 | 0.522 | 0.198 |
| 5 | 533.5 | 0.491 | 0.182 |
| 6 | 645.0 | 0.508 | 0.104 |
| 7 | 754.6 | 0.459 | 0.081 |

Figure 9. Theoretical and Experimental Frequency Responses for Third Test

## 5.4. TRANSIENT PRESSURE EXCITATION WITH CONSTANT ACOUSTIC IMPEDANCE

The transient response of the system was next verified. The experiment was initiated by attaching a pulse generator to the amplifier in order to excite the speaker. The electrical impulse produced was converted to one cycle of sine wave acoustic energy at approximately 500 Hz (Figure 10). The system input pressure and response pressure were measured by Bruel and Kjaer Type 4166 half-inch microphones attached to an Apple Macintosh IIx computer running National Instruments Labview software and an NB-MIO-16L analog-to-digital converter. The length of the duct in this test was 2.44 m (8.00 ft), and the response was measured at $x = 0.792$ m (2.60 ft). The packing foam used in the first and second experiments was also used here to provide a nonzero acoustic impedance at the end of the duct. The measured time domain experimental data were compared to the theoretical model response. Only the real part of $K$ was used in the theoretical formulation.

Figure 11 is a plot of the experimental data and theoretical state-space model. The solid line shows the experimental data and the dashed line depicts the theoretical model. The theoretical model response was computed using a fifth-order Adams' integration method with 51 states. The forcing function in the Adams' integration routine was the measured system input at $x = 0$. The integration step size was $\Delta t = 0.000035$ seconds, which matched the Labview sampling rate of 28571 Hz. There is an excellent match between the theoretical model and experimental data from $t = 0$ to $t = 0.015$ seconds. After that, the experimental data and theoretical prediction deviate because the propagating pressure pulse is reflected off the now inactive speaker and is affected by its impedance. The theoretical model does not account for impedance at the inactive speaker (zero velocity); however, Figures 6, 8, and 9 illustrate that an active speaker used in this experiment has little effect on the impedance at the source end ($x = 0$) for the test frequencies used here.

Figure 10. System Pressure Input at $x = 0$



Figure 11. Transient Response of Duct at $x = 0.792$ m

# 6. ACOUSTIC IMPEDANCE MEASUREMENT

The acoustic impedance $K$ of the termination end can be determined at each duct resonance from the eigenvalue corresponding to that resonance. This computation assumes that the eigenvalues of the system are known. Measuring these duct system eigenvalues is discussed below. Directly solving for $K$ in terms of $\Lambda$ is very difficult; therefore an intermediate variable $\beta$ is introduced to simplify the acoustic impedance computation. The variable $\beta_n$ is related to the $n$th eigenvalue $\Lambda_n$ from equations (10) and (12) as

$$\text{Re}(\Lambda_n) + i\,\text{Im}(\Lambda_n) = \frac{c}{2L}\log_e\left[\text{Re}(\beta_n) + i\,\text{Im}(\beta_n)\right] - \frac{n\pi ci}{L} , \tag{32}$$

where Re( ) denotes the real part, Im( ) denotes the imaginary part, and the subscript "$n$" denotes the $n$th term. Equation (32) is now divided into two parts, one equating the real coefficients and the other equating the imaginary coefficients. The complex logarithm on the right-hand side is rewritten as

$$\log_e\left[\text{Re}(\beta_n) + i\,\text{Im}(\beta_n)\right] = \log_e|\beta_n| + i\,\text{arg}(\beta_n) , \tag{33}$$

where $|\beta_n|$ is the magnitude of $\beta_n$ and $\text{arg}(\beta_n)$ is the argument of $\beta_n$, i.e., the arctangent of $\left[\text{Im}(\beta_n) / \text{Re}(\beta_n)\right]$.

The intermediate variable $\beta_n$ is now solved for in terms of the real and imaginary parts of the eigenvalues. The real part of $\beta_n$ is

$$\text{Re}(\beta_n) = \pm\left[\frac{\exp\left(\dfrac{4L\,\text{Re}(\Lambda_n)}{c}\right)}{1 + \tan^2\left(\dfrac{2Ld_n}{c}\right)}\right]^{\frac{1}{2}} , \tag{34a}$$

where

$$d_n = \text{Im}(\Lambda_n) - \frac{nc\pi}{L} . \tag{34b}$$

The sign of the right-hand side of equation (34a) is determined by

26

$$\text{sgn}[\text{Re}(\beta_n)] = \begin{cases} +1 \text{ if } 0 \le |\Delta| \le 0.25 \\ -1 \text{ if } 0.25 \le |\Delta| \le 0.50 \end{cases}, \tag{35a}$$

where

$$\Delta = d_n \left( \frac{L}{c\pi} \right). \tag{35b}$$

If the value of $\Delta$ is less than -0.5 or greater than 0.5, the eigenvalue index $n$ is incorrect and corresponds to an eigenvalue other than the $n$th one. The value of $n$ must then be changed to produce a $\Delta$ between -0.5 and 0.5, which will correspond to the correct eigenvalue index. Once $\text{Re}(\beta_n)$ is found, $\text{Im}(\beta_n)$ can be solved using

$$\text{Im}(\beta_n) = \text{Re}(\beta_n) \tan\left( \frac{2Ld_n}{c} \right), \tag{36}$$

where $\text{Re}(\beta_n)$ is given in equation (34).

Use of equations (10) and (32) now allows the term $(1-K)/(1+K)$ to be equated to the intermediate variable $\beta_n$ as

$$\text{Re}(\beta_n) + i\,\text{Im}(\beta_n) = \frac{1 - \text{Re}(K_n) - i\,\text{Im}(K_n)}{1 + \text{Re}(K_n) + i\,\text{Im}(K_n)}, \tag{37}$$

where $\text{Re}(K_n)$ is the real part of $K$ and $\text{Im}(K_n)$ is the imaginary part of $K$ corresponding to the $n$th eigenvalue. Breaking equation (37) into two equations and solving for $K_n$ as a function of $\beta_n$ yield the acoustic impedance as

$$\text{Re}(K_n) = \frac{1 - [\text{Re}(\beta_n)]^2 - [\text{Im}(\beta_n)]^2}{[\text{Re}(\beta_n) + 1]^2 + [\text{Im}(\beta_n)]^2} \tag{38}$$

and

$$\text{Im}(K_n) = \frac{-2\,\text{Im}(\beta_n)}{[\text{Re}(\beta_n) + 1]^2 + [\text{Im}(\beta_n)]^2}. \tag{39}$$

Acoustic impedance measurement $K_n$ represents the acoustic impedance at the $n$th resonant frequency.

Because steady-state eigenvalue measurements are amplitude dominated rather than phase dominated, the impedance measurement technique developed here does not require phase-matched microphones, nor does it require compensation for phase-mismatched microphones. Phase mismatch in the microphones is neglected since the measurements are made at a duct resonant frequency; i.e., the measurements are made when the system phase angles are changing rapidly through 180 degrees. Microphones operating under 500 Hz rarely have a phase error greater than 5 degrees (Bruel and Kjaer, 1982). The distance between the microphones is also not critical because the duct eigenvalues are independent of measurement location, unlike in previous methods (Seybert and Ross, 1977; Chung and Blaser, 1980a, 1980b) where microphone spacing is a required parameter in the analysis and phase-matched microphones (or a compensation function) are necessary because wave propagation across the microphones is detected. The computation of acoustic impedance from duct eigenvalues is a closed-form solution. Thus, errors in the method developed here are only a function of errors associated with measuring the eigenvalues of the duct, the duct length, and the speed of sound. In addition, because this method uses the input microphone as an amplitude reference, the excitation speaker does not require a flat response around the frequency of interest since the response is normalized by the pressure input reference when the fast Fourier transform is computed.

The 5423A Structural Dynamics Analyzer used in this research is capable of providing a number of real-time analyses, including the determination of the transfer function (frequency response) of a system and calculation of the corresponding eigenvalues. The analyzer accomplishes this by curve fitting a single-mode vibration model (two first-order states) to the experimental data. Included in the single-mode vibration model is compensation for other modes, which may be overlapping at that particular frequency. During the curve-fitting process, the real and imaginary parts of the eigenvalues are calculated. Although it is beyond the scope of this paper to describe the process, modal parameter extraction from the transfer function of the system is a common function of

commercial fast Fourier analyzers (Hewlett Packard, 1979; Structural Dynamics Research Corporation, 1983).

## 7. CONCLUSIONS

The modal decomposition of an impedance tube was theoretically demonstrated and experimentally verified. The new model incorporates pressure at the end or velocity input in the spatial domain, as well as unknown impedance at the termination end. The model is valid for both steady-state and transient responses. Several experiments have shown that the model is extremely accurate. The acoustic impedance at the termination end could be determined by using the eigenvalues from the steady-state experiments.

## 8. REFERENCES

The American Society for Testing and Materials, 1985a, "Standard Test Method for Impedance and Absorption of Acoustical Materials by the Impedance Tube Method," Annual Book of ASTM Standards, Designation: C 384-85, Vol. 04-06, pp. 144-156.

The American Society for Testing and Materials, 1985b, "Standard Test Method for Impedance and Absorption of Acoustical Materials Using a Tube, Two Microphones, and a Digital Frequency Analysis System," Annual Book of ASTM Standards, Designation: E 1050-85a, Vol. 04-06, pp. 910-917.

Bruel and Kjaer, 1982, "Condenser Microphones and Microphone Preamplifiers," Bruel and Kjaer Instruments, Inc., Naerum, Denmark.

Chung, J. Y., and Blaser, D. A., 1980a, "Transfer Function Method of Measuring In-Duct Acoustic Properties. I. Theory," *Journal of the Acoustical Society of America,* Vol. 68(3), pp. 907-913.

Chung, J. Y., and Blaser, D. A., 1980b, "Transfer Function Method of Measuring In-Duct Acoustic Properties. II. Experiment," *Journal of the Acoustical Society of America,* Vol. 68(3), pp. 914-921.

Davis, D. D., Jr., Stokes, G. M., Moore, D., and Stevens, G. L., Jr., 1954, "Theoretical and Experimental Investigation of Mufflers With Comments on Engine Exhaust Design," NACA Report 1192, National Advisory Committee for Aeronautics.

Doak, P. E., 1973a, "Excitation, Transmission and Radiation of Sound From Source Distributions in Hard-Walled Ducts of Finite Length (II): The Effects of Duct Length," *Journal of Sound and Vibration*, Vol. 31(2), pp. 137-174.

Doak, P. E., 1973b, "Excitation, Transmission and Radiation of Sound From Source Distributions in Hard-Walled Ducts of Finite Length (I): The Effects of Duct Cross-Section Geometry and Source Distribution Space-Time Pattern," *Journal of Sound and Vibration*, Vol. 31(1), pp. 1-72.

Hewlett-Packard, 1979, "User's Guide, 5423A Structural Dynamics Analyzer," Hewlett-Packard Company, Santa Clara, California.

Morse, P. M., and Ingard, K. U., 1968, *Theoretical Acoustics*, McGraw-Hill Book Company, New York, pp. 469-471.

Pierce, A. D., 1981, *Acoustics: An Introduction to Its Physical Principles and Applications*, McGraw-Hill Book Company, New York, pp. 111-113 and p. 321.

Rayleigh, J. W. S., 1878, *The Theory of Sound, Volume II*, Dover Publications, New York, pp. 49-68.

Seto, W. W., 1971, *Theory and Problems of Acoustics*, McGraw-Hill Book Company, New York.

Seybert, A. F., and Ross, D. F., 1977, "Experimental Determination of Acoustic Properties Using a Two-Microphone Random-Excitation Technique," *Journal of the Acoustical Society of America*, Vol. 61, pp. 1362-1370.

Snowdon, J. C., 1971, "Mechanical Four Pole Parameters and Their Application," *Journal of Sound and Vibration*, Vol. 15, pp. 307-323.

Spiekermann, C. E., and Radcliffe, C. J., 1988a, "Decomposing One-Dimensional Acoustic Response Into Propagating and Standing Waves," *Journal of the Acoustical Society of America,* Vol. 84(4), pp. 1536-1541.

Spiekermann, C. E., and Radcliffe, C. J., 1988b, "Stripping One-Dimensional Acoustic Response Into Propagating and Standing Wave Components," *Journal of the Acoustical Society of America,* Vol. 84(4), pp. 1542-1548.

Structural Dynamics Research Corporation, 1983, "User Manual for MODAL ANALYSIS 8.0," Structural Dynamics Research Corporation, Milford, Ohio.

Swinbanks, M. A., 1973, "The Active Control of Sound Propagation in Long Ducts," *Journal of Sound and Vibration,* Vol. 27(3), pp. 411-436.

Tichy, J., Warnaka, G. E., and Poole, L. A., 1984, "A Study of Active Control of Noise in Ducts," *Journal of Vibration, Acoustics, Stress, and Reliability in Design,* Vol. 106, pp. 399-404.

Trinder, M. C. J., and Nelson, P. A., 1983, "Active Noise Control in Finite Length Ducts," *Journal of Sound and Vibration,* Vol. 89(1), pp. 95-105.

# INITIAL DISTRIBUTION LIST

| Addressee | No. of Copies |
|---|---|
| Defense Technical Information Center | 12 |